

Manuscript

Senescent stromal cells promote cancer resistance through SIRT1 loss-potentiated overproduction of small extracellular vesicles

Liu Han¹, Qilai Long², Shenjun Li³, Qixia Xu⁴, Boyi Zhang¹, Xuefeng Dou¹, Min Qian¹,
Yannasittha Jiramongkol⁵, Jianming Guo², Liu Cao⁶, Y. Eugene Chin⁷, Eric W.-F. Lam⁵,
Jing Jiang⁸ and Yu Sun^{1,4,9}

¹ CAS Key Laboratory of Tissue Microenvironment and Tumor, Shanghai Institute of Nutrition and Health, Shanghai Institutes for Biological Sciences, University of Chinese Academy of Sciences, Chinese Academy of Sciences, Shanghai 200031, China.

² Department of Urology, Zhongshan Hospital, Fudan University, Shanghai 200032, China.

³ Non-clinical Research Department, RemeGen, Ltd. Yantai, Shandong 264005, China.

⁴ Institute of Health Sciences, Shanghai Jiao Tong University School of Medicine & Shanghai Institutes for Biological Sciences, Chinese Academy of Sciences, Shanghai 200031, China.

⁵ Department of Surgery and Cancer, Imperial College London, London, W12 0NN, UK.

⁶ Key Laboratory of Medical Cell Biology, China Medical University, Shenyang 110122, China.

⁷ Institute of Biology and Medical Sciences, Soochow University Medical College, 199 Renai Road, Suzhou, Jiangsu 215123, China.

⁸ Department of Pharmacology, Binzhou Medical University, Yantai, Shandong 264003, China.

⁹ Department of Medicine and VAPSHCS, University of Washington, Seattle, WA 98195, USA.

Note: Supplementary data for this article are available at Cancer Research online (<http://cancerres.aacrjournals.org/>).

L. Han and Q. Long contributed equally to this article.

Corresponding Author: Yu Sun, Shanghai Institutes for Biological Sciences, Chinese Academy of Sciences, 320 Yueyang Road, Shanghai 200031, China. Phone: 86-21-54923302; Fax: 86-21-54923302; E-mail: sunyu@sibs.ac.cn

Running Title: Senescent Stromal Cells Drive Cancer Resistance via sEVs

Keywords: Cellular senescence, stromal cell, cancer resistance, SIRT1, small extracellular vesicle

Conflict of Interest Statement: The authors declare no potential conflicts of interest.

Abstract

Cellular senescence is a potent tumor-suppressive program that prevents neoplastic events. Paradoxically, senescent cells develop an inflammatory secretome, termed the senescence-associated secretory phenotype (SASP), which is implicated in age-related pathologies including cancer. Here we report that senescent cells actively synthesize and release small extracellular vesicles (sEVs) with a distinctive size distribution. Mechanistically, SIRT1 loss supported accelerated sEV production despite enhanced proteome-wide ubiquitination, a process correlated with ATP6V1A downregulation and defective lysosomal acidification. Once released, senescent stromal sEVs significantly altered the expression profile of recipient cancer cells and enhanced their aggressiveness, specifically drug resistance mediated by expression of ATP binding cassette subfamily B member 4 (ABCB4). Targeting SIRT1 with agonist SRT2104 prevented

development of cancer resistance by restraining sEV production by senescent stromal cells. In clinical oncology, sEVs in peripheral blood of posttreatment cancer patients were readily detectable by routine biotechniques, presenting an exploitable biomarker to monitor therapeutic efficacy and predict long-term outcome. Together, this study identifies a distinct mechanism supporting pathological activities of senescent cells and provides a potent avenue to circumvent advanced human malignancies by co-targeting cancer cells and their surrounding microenvironment, which contributes to drug resistance via secretion of sEVs from senescent stromal cells.

Significance: Senescent stromal cells produce a large number of sEVs to promote cancer resistance in therapeutic settings, a process driven by SIRT1 decline in stromal cells and ABCB4 augmentation in cancer cells.

Introduction

Cytotoxic chemotherapy represents an effective modality for cancer treatment, inducing clinical responses associated with a significantly lowered risk of recurrence, but only in a limited fraction of patients (1-3). As selection of genes accurately predicting therapeutic responses might improve cancer outcomes, gene signatures aimed at predicting responses to specific anticancer agents and minimizing drug resistance are being actively evaluated (4). Multiple studies have reported side-effects generated by local and systemic treatments, and their therapeutic benefits may be restrained by tumor-promoting host responses induced by certain forms of cytotoxicity (5). Development of innate and/or acquired resistance are among the major mechanisms underlying diminished responsiveness to anticancer regimens, as disease relapse after an initial

response can occur as a result of systemic release of multiple soluble factors, which frequently remodel the treatment-damaged tumor microenvironment (TME) (6,7).

Cellular senescence is a state of cell cycle arrest that occurs upon exposure of cells to different stresses, usually resistant to cell death induction. While cellular senescence is beneficial for a few physiological events such as tissue repair, wound healing and embryogenesis (8-10), it accelerates organismal aging and is responsible for age-related disorders including cancer (11,12). Senescent cells synthesize and secrete a plethora of extracellular proteins, covering growth factors, cytokines, chemokines and proteases, a phenomenon referred to as the SASP (13-15). Expression of most of the SASP components are regulated by kinases including TAK1, p38, mTOR and Jak2/Stat3, all of which indeed converge on the NF- κ B complex and the c-EBP/ β family of transcription factors (16). By means of the SASP expression, senescent cells remodel the local tissue via paracrine mechanisms and recruit immune cells in aging tissues (17). In response to damage signals, degradation of the nuclear lamina and elimination of the major structural component lamin B1 not only enhance histone depletion and chromatin remodeling but also forms microtubule-associated protein light chain 3 (LC3/ATG8)-containing cytoplasmic chromatin fragments (18,19). If not eliminated via exosome secretion, such chromatin fragments can activate the cyclic GMP-AMP synthase (cGAS) and stimulator of interferon- γ (IFN- γ) genes (STING) response, further promoting expression of the SASP and type I interferons (IFNs) (20,21).

Extracellular vesicles (EVs) are membranous vesicles released by almost all cell types and contain a lipid bilayer that protects the luminal contents of proteins, nucleic acids, lipids and metabolites against harsh environmental conditions (22). According to their distinctive biogenesis and release modes, EVs can be categorized as exosomes, microvesicles (MVs) and

apoptotic bodies (ABs) (23). The cargos packaged within or associated with the EVs can reflect the pathophysiological state of host cells (24). However, the capacity of senescent cell-derived EVs in orchestrating intercellular communications within the TME and changing pathological track under therapeutic settings, remain largely unexplored. To this end, we investigated the biogenesis mechanisms of EVs generated by senescent human stromal cells developing the SASP, and disclosed that EVs can shape acquired resistance of cancer cells to anticancer treatments. We further demonstrated the feasibility of modulating EV production to control therapeutic resistance acquired from the treatment-damaged TME, thus presenting a potent avenue to improve therapeutic efficacy by harnessing senescent cell-derived EVs.

Materials and Methods

Cell culture

Primary normal human prostate stromal cell line PSC27 and breast stromal cell line HBF1203 were derived from fresh surgical samples and maintained in stromal complete medium as described (25). Stromal cells at a passage number of 2~5 were employed for experimental assays. Prostate cancer cell lines PC3, DU145, LNCaP, M12 and breast cancer cell line MDA-MB-231 (ATCC) were routinely cultured with RPMI1640 (10% FBS). All cell lines were tested negative for mycoplasma contamination and authenticated with STR assays.

***In vitro* treatments and senescence appraisal**

PSC27 cells were grown until 80% confluent (CTRL) and treated with bleomycin (50 µg/ml, BLEO) for 12 h. After treatment, the cells were rinsed thrice with PBS and allowed to stay for 7-10 d in media. Alternatively, HBF1203 cells were treated with doxorubicin (10 µM,

DOX) for 12 h to induce senescence. To examine cellular senescence, SA- β -Gal staining and BrdU incorporation were performed. DNA-damage extent was evaluated by immunostaining for γ H2AX or p-53BP1 foci by following a 4-category counting strategy as formerly reported (25). Random fields were chosen to show SA- β -gal positivity, BrdU incorporation or DDR foci, and quantified using CellProfiler (<http://www.cellprofiler.org>).

Vectors, viruses, infection and transcript assays

Lentiviral vector pLKO.1-Puro (Addgene) was used to clone small hairpin RNAs (shRNAs), including those targeting human SIRT1 (1# sense strand 5'-CCGGTGC GGGAATCAAAGGATAATTCTCGAGAATTATCCTTTGGATTCCCGCTTTT TG-3'; 2# sense strand 5'-CCGGTGCTGATGAACCGCTTGCTATCCTCGAGGATAGCAAGCGGTTTCATCAGCTTTT TG-3'), human ABCB4 (#1 sense strand 5'-CCGGCCAATCGAGAATCAGCTATTACTCGAGTAATAGCTGATTCTCGATTGGTTTTT G-3'; #2 sense strand 5'-CCGGCCGAGCATTCTCTGATCCATTCTCGAGAATGGATCAGAGAATGCTCGGTTTTT G-3') and human miR-34a (Accession NR_029610) (#1 sense strand 5'-CCGGAGCAATCAGCAAGTATACTGCCCTACTCGAG TAGGGCAGTATACTTGCTGATTGCTTTTTTTG-3'; 2# sense strand 5'-CCGGAATCAGCAAGTATACTGCCCTAGAA CTCGAGTTCTAGGGCAGTATACTTGCTGATTTTTTTG-3'). For each target gene, the scramble sense strand was 5'-CCGGTTAGCGACTAAACACATCAATTCAAGAGATTGATGTGTTTAGTCGCTATTTTTT G-3'. Lentiviral vector pLenti-CMV-Puro-DEST (Invitrogen) was used for generation of

expression constructs for target genes. Upon production by 293FT cells, lentiviral titers were adjusted to infect ~90% of cells. Stromal cells were infected overnight in the presence of polybrene (8 $\mu\text{g}/\text{ml}$), allowed to recover for 48 h and selected for 72 h before analysis. For expression of target genes in either stromal or epithelial cells, total RNA was prepared and subject to qRT-PCR assays (primers listed in Supplementary Table S1).

Immunoblotting and immunofluorescence

Proteins were separated using SDS-PAGE gels and transferred onto nitrocellulose membranes. The blots were blocked with 5% nonfat dry milk at room temperature for 1 h and incubated overnight at 4°C with desired primary antibodies, followed by incubation with HRP-conjugated secondary antibodies (Santa Cruz) and membrane exposure with ECL reagent (Millipore).

For immunofluorescence staining, cells were cultured in dishes and pre-seeded for at least 24 h on coverslips. Cells were fixed with 4% paraformaldehyde in PBS, blocked with 5% normal goat serum and incubated with primary antibodies. Alexa Fluor 488 or 594-conjugated secondary antibodies (Invitrogen, 1:400) were used. Nuclei were stained with Hoechst 33342 before fluorescence imaging (Nikon Eclipse Ti S). Alternatively, a confocal microscope (Zeiss LSM 780) was applied to acquire confocal images (antibodies listed in Supplementary Table S2).

Preclinical studies

All animals were maintained in a specific pathogen-free (SPF) facility, with NOD/SCID (Nanjing Biomedical Research Institute of Nanjing University) mice at an age of approximately 6 weeks (~20g body weight) used. Each group comprised 10 mice, and xenografts were

subcutaneously implanted at the hind flank. Stromal cells (PSC27) were mixed with cancer cells (PC3) at a ratio of 1:4 (250,000 stromal cells admixed with 1,000,000 cancer cells to make tissue recombinants). Animals were sacrificed at end of the 8th week after tumor xenografting as previously described (26).

For chemoresistance studies, animals received subcutaneous implantation of tissue recombinants and were given standard laboratory diets for 2 weeks to allow tumor uptake and growth initiation. Starting from the 3rd week (tumors reaching 4-8 mm in diameter), MIT (0.2 mg/kg doses) or vehicle control was administered via intraperitoneal injection on the 1st day of 3rd, 5th and 7th weeks, respectively. Upon completion of the 8-week regimen, animals were sacrificed, with tumor volumes recorded and tissues processed for histological evaluation. For SIRT1 activation, SRT2104 (Selleck) was dissolved in suspension (30% PEG 400/0.5% Tween 80/5% Propylene glycol at 30 mg/ml), administered via oral gavage at a 100 mg/kg dose every other week, starting from the 1st day of the 3rd week after xenograft implantation and provided either alone or together with MIT, until completion of the 8-week regimen.

All animal experiments were performed in compliance with NIH Guide for the Care and Use of Laboratory Animals (National Academies Press, 2011) and the ARRIVE guidelines, and were approved by the Institutional Animal Care and Use Committee (IACUC) of Shanghai Institutes for Biological Sciences, Chinese Academy of Sciences.

Clinical investigation

Randomized control trial (RCT) protocols and all experimental procedures were approved by the Ethics Committee and Institutional Review Board of Shanghai Jiao Tong University School of Medicine and Zhongshan Hospital of Fudan University. Relevant methods were

applied following official guidelines. Written informed consent was obtained from all subjects, with experiments conformed to principles set out in the WMA Declaration of Helsinki and the Department of Health and Human Services Belmont Report.

Statistical analyses

All *in vitro* experiments were performed in triplicates, and animal studies were conducted with $n \geq 8$ mice per group. Animals were distributed into groups of equal body weight, and no animals were excluded from analysis. Sample sizes were estimated based on an 80% power to detect a 50% reduction in tumor volumes observed in mice subject to chemotherapy and/or targeted therapy compared with control mice, accepting a type I error rate of 0.05.

When comparing two conditions, Student's *t* tests with Mann-Whitney's tests were used to determine statistical significance. More than two comparisons were made using one-way ANOVA followed by Dunn's or Tukey's post hoc tests. Two-way ANOVA with Bonferroni correction was used for grouped analysis. Nonlinear dose-response fitting curves were generated with GraphPad Prism 7.0. *P* values < 0.05 were considered significant, and two-sided tests were performed. Unless otherwise indicated, all data in the figures were presented as mean \pm SD. Univariate and multivariate Cox proportional hazards model analysis were performed with statistical software SPSS.

Data availability

The raw RNA-seq data have been deposited in the Gene Expression Omnibus database (accession codes GSE128282 and GSE128405). The authors declare that all other data supporting the findings of this study are available within the article or its Supplementary Materials and from the corresponding author upon reasonable request.

Results

Senescent stromal cells generate an increased number of EVs with distinct size distribution

As stromal cells represent the major non-cancerous mesenchymal components providing structural architecture within the tissue of most solid tumors, we chose to employ a primary normal human prostate stromal cell line, namely PSC27, to initiate the study. Composed of predominantly fibroblasts but with a minor percentage of non-fibroblast cell lineages including endothelial cells and smooth muscle cells, PSC27 cells are primary in nature and develop a typical SASP after exposure to stressful insults such as cytotoxic chemotherapy or ionizing radiation (25-27). We treated these cells with a pre-optimized sub-lethal dose of bleomycin (BLEO), resulting in enhanced senescence-associated β -galactosidase (SA- β -Gal) staining positivity, decreased BrdU incorporation, and elevated DNA damage foci several days afterwards (Supplementary Fig. S1A-C). Data from Illumina sequencing (RNA-seq) indicated that PSC27 cells were strongly expressing multiple SASP factors including but not limited to CXCL8, CCL20, CSF3, IL-1 α and CCL3 after treatment (Supplementary Fig. S1D). We isolated stromal cell-derived vesicles with sequential ultracentrifugation before assessment of their size and distribution. Strikingly, quantitative nanoparticle tracking analysis (NTA) showed that the number of senescent (SEN) PSC27 cell-released vesicles between 30 nm and 1.0 μ m, a size range characterized of major eukaryotic EV subtypes including exosomes and MVs (28), was approximately 7 times of their proliferating (PRO) counterparts (Fig. 1A). Further, we noticed a substantial difference of EV size distribution between PRO and SEN stromal cells. In contrast to EVs from PRO cells, which were mainly enriched at 72, 102, 121 and 170 nm, EVs from SEN cells displayed an evident re-distribution in particle diameter, as reflected by several major peaks

at 33, 47, 64, 122, 156, 182, 266 and 314 nm, respectively, although in each case the refereed EVs fell in the category of small EVs (sEVs) as defined by recent literatures and excluding their identity as other EV subtypes such as ABs (28,29) (Fig. 1B). The average size shifted from 116 nm to 161 nm, with a statistical significance between PRO and SEN cell-derived sEVs, a pattern suggesting potential difference of their cargo contents (Fig. 1C-D). Though there was a small number of EVs displaying sizes beyond such a principal window, they accounted for a limited percentage of overall stromal EVs and were not the main focus of subsequent investigations.

Preliminary in-gel analysis indicated that protein components of sEVs from PRO and SEN cells apparently differ from each other, when sample loading was normalized to the number of sEVs (Fig. 1E). However, when loading was normalized to the number of parental cells that secreted these sEVs, we noticed substantially enhanced amounts of sEV protein cargoes (Fig. 1F). The findings were supported by immunoblots, which suggested that expression of sEV-specific markers such as syntenin-1, TSG101 and ALIX was markedly increased in total sEV lysates upon cellular senescence (Fig. 1G). We then analyzed the whole lysates of parental cells, and found considerably elevated expression of sEV markers in SEN cells, in contrast to PRO samples (Fig. 1H). Upon immunofluorescence (IF) staining, we found the expression levels of CD63 (a tetraspanin protein) and TSG101 apparently enhanced in SEN cells, implying the possibility of active synthesis of sEVs in MVBs (Fig. 1I). Electron microscopy imaging showed expanding MVBs with an increase in both volume and the number of their internal vesicles in SEN cells, relative to their proliferating counterparts (Fig. 1J-K). Indeed, there was a concomitant upregulation of the vast majority of sEV-associated molecules as indicated by transcript assays, although the expression level of SMPD2/3, two neutral sphingomyelinases (nSMases) associated with biogenesis of both sEVs and MVs, appeared increased, as well (Fig.

1L). Further analysis with successive differential ultracentrifugation of pellets from conditioned media, a strategy that effectively separates sEVs from MVs (14,000 g and 100,000 g of sedimentation, respectively) (30), indicated enhanced secretion of sEVs by SEN cells, while MV release remained largely unchanged, implying engagement of a mechanism specifically responsible for production of sEVs, but not all EV subtypes (Fig. 1M). Notably, appearance of such a distinct expression pattern was accompanied by pronounced upregulation of several hallmark SASP factors including but not limited to IL6, IL8, IL1 α , WNT16B, MMP3 and GM-CSF (Fig. 1L).

To validate the data, we chose HBF1203, another stromal cell line which was isolated from human breast tissue and consists mainly of fibroblasts upon primary culture. We treated HBF1203 with doxorubicin (DOX), a chemotherapeutic agent frequently used in breast cancer clinics. The results suggested that senescence-associated changes including those in cell phenotypes, sEV marker and SASP factor expression, and sEV production, can be readily reproduced in these cells (Supplementary Fig. S1E-J). Thus, these data uncover a common feature potentially shared by stromal cells of multiple tissue and/or organ origin.

SIRT1 decline supports deficient lysosomal acidification and enhanced sEV biogenesis via ATP6V1A downregulation

Given the substantial change of the number and cargo composition of sEVs generated by stromal cells upon senescence, we interrogated the mechanism supporting these alterations. It was suggested that dysfunctional lysosome or autophagy can promote EV biogenesis through modifying the fate of MVBs, the direct cytoplasmic source of exosomes (31,32). A recent study further revealed that reduced SIRT1 expression in breast cancer cells can modify lysosomal

activity, resulting in enhanced release of exosomes from these cells and significant changes in their exosome composition (33).

We first assessed the expression level of human SIRT family, a group of NAD⁺-dependent deacetylases, in proliferating and senescent cells. Whole transcriptomic analysis by RNA-seq suggested that all 7 members of this family were ubiquitously downregulated, although a statistical significance was observed mainly in SIRT1 and SIRT2 (Fig. 2A-B). Downregulation of SIRT1/2 was accompanied by upregulation of IL8 and MMP3, hallmark SASP factors (Fig. 2C). Upon cellular senescence, DNA damage-associated concomitant decline of SIRT1/2 was indeed also observed in a human primary fibroblast line BJ (34), essentially supporting our data. SIRT1 regulates diverse cellular targets and correlates with organismal aging, while SIRT2 has been reported to be marker of cellular senescence in certain cancer types such as osteosarcoma (35,36). Although loss of SIRT1 enhances the secretion of exosomes by breast cancer cells, whether or not this occurs in stromal cells remains unclear. In our work, knockdown of SIRT1 with small hairpin RNAs (shRNAs) caused significant upregulation of not only the typical sEV markers including TSG101, Syntenin-1, ALIX and tetraspenins (CD9/63/81), but also downregulation of HSP70 (HUGO symbol HSPA4), the latter reported to be responsible for accumulation of ubiquitinated proteins in mammalian cells (37) (Fig. 2D). However, expression of IL6, IL8 and MMP3, a set of canonical SASP factors, remained unaffected upon SIRT1 depletion, suggesting that SIRT1 loss itself was insufficient to induce the SASP development (Fig. 2D). We further noticed that DNA damage treatment caused reduction of HSP70, accompanied by increased TSG101, IL8 and MMP3, as evidenced by both transcript and protein assays (Supplementary Fig. S2A-B). To the contrary, exogenous expression of HSP70 caused

decreased levels of TSG101 and ALIX, suggesting a negative correlation between HSP70 expression and sEV production in these cells (Supplementary Fig. S2C).

The SASP is functionally modulated by several master regulators, including the NF- κ B complex, which controls both cell-autonomous and non-cell-autonomous activities of cellular senescence program (38). However, whether SIRT1 loss is subject to NF- κ B regulation remains unknown. We used Bay 11-7082 (BAY) to treat PSC27 cells, and found that SIRT1 decrease appeared reversed upon NF- κ B suppression, in sharp contrast to many of the SASP factors such as IL8 and MMP3 whose expression was markedly diminished after BAY treatment (39) (Supplementary Fig. S2D). More importantly, NF- κ B inhibition substantially reduced expression of TSG101, ALIX, CD63 and CD81 after BLEO treatment, indicating compromised sEV biogenesis even in the setting of DNA damage. We next asked the mechanism underlying SIRT1 reduction in damaged cells. As microRNA 34a (miR-34a) can inhibit SIRT1 expression through targeting the 3'UTR of SIRT1 upon cellular stress (40), we first examined the expression profile of miR-34a. Of note, miR-34a was significantly upregulated in PSC27 cells upon genotoxic treatment (Supplementary Fig. S2E). Further analysis indicated that miR-34a expression was mainly driven by NF- κ B, while targeting miR-34a essentially prevented SIRT1 decline in damaged stromal cells (Supplementary Fig. S2E-F). Further, chemical inhibition of the poly(ADP-ribose) (PAR) polymerase 1 (PARP1), an enzyme functionally involved in cellular senescence, SASP development and NF- κ B activation upon DNA damage events (41), failed to affect the expression pattern of either SIRT1 or ALIX, suggesting double strand breaks, which underlie ATM- and/or ATR-dependent DNA damage response (DDR), instead of single strand lesions, are indeed responsible for reduced SIRT1 expression and enhanced sEVs biogenesis in DNA-damaged cells (Supplementary Fig. S2G).

To substantiate the correlation of SIRT1 with sEV production, we used suberoylanilide hydroxamine acid (SAHA) and nicotinamide (NAM), a pan-histone deacetylase (HDAC) inhibitor (at least against HDAC 1/2/4) and a SIRT-specific inhibitor (against HDAC3), respectively, to treat PSC27 cells. Immunoblots indicated that expression of SIRT1, IL8 and MMP3 remained unchanged, HSP70 decreased, while sEV markers including ALIX and CD63 increased when cells were treated by either agent even in the absence of DNA damage, suggesting that the activity SIRTs and other HDACs responsible for deacetylation of certain targets is critical for the synthesis of sEV-central molecules, but not for development of the SASP (Supplementary Fig. S2H). To the contrary, activation of SIRT1 by SRT2104, a selective SIRT1 activator, substantially diminished sEV signals and protein ubiquitination, alterations caused by NAM, regardless of DNA damage treatment, although expression of TSG101, ALIX, CD63, IL8 and MMP3 was remarkably higher when cells were exposed to BLEO (Fig. 2E). Thus, SIRT1 is a critical but negative modulator of sEV biogenesis, and functionally responsible for restrained proteome-wide ubiquitination.

Enhanced production or reduced degradation of ubiquitinated proteins by the proteasome or autophagy can result in elevated amount of ubiquitinated proteins (37). To assess proteasome integrity in damaged cells, we used the proteasome inhibitor MG132 to treat PSC27, and found pronouncedly increased protein ubiquitination after genotoxic exposure (Supplementary Fig. S2I). Upon treatment with Bafilomycin A1, a selective inhibitor of the late phase of autophagy that prevents maturation of autophagic vacuoles by targeting vacuolar H⁺-ATPases (V-ATPases) and restraining fusion between autophagosomes and lysosomes (42), we noticed elevated levels of autophagy markers p62 and LC3 II, regardless of cell exposure to genotoxic stress, indicating the integrity of autophagy even with SIRT1 loss and protein ubiquitination in these senescent

cells (Supplementary Fig. S2J). Upon treatment by cycloheximide (CHX), a protein synthesis inhibitor, we observed markedly reduced protein ubiquitination, but not SIRT1 level (Supplementary Fig. S2K). The total protein of EGFR, a transmembrane receptor subject to polyubiquitination and proteasome-mediated degradation (43), remained largely unaffected when BLEO-damaged cells were exposed to CHX. Indeed, the relative constant amount of EGFR protein was in line with reduced level of ubiquitination in CHX-treated cells, which presumably had decreased capacity in mediating protein turnover. Thus, SIRT1 was not subject to significant protein degradation in senescent cells, with its decrease mainly attributable to downregulation of SIRT1 starting from the transcription level, although accumulation of ubiquitinated proteins implies functional deficiency of lysosomes.

We next interrogated whether SIRT1 loss affects lysosomal function by assaying the pH of lysosomes with LysoSensor yellow/blue dextran ratiometric probe, which accumulates in acidic organelles as the result of protonation. In contrast to PRO cells whose lysosome pH was 4.8, consistent with the reported pH of physiologically normal lysosomes (44), SEN cells exhibited a lysosomal pH approaching 6.0 (Fig. 2F). To determine whether the increase of SEN cell lysosomal pH results from a defective proton pump, we performed lysosomal re-acidification assays by first enhancing the pH by Bafilomycin A1-treatment, then adding LysoTracker to assess the rate of lysosomal pH recovery. While the pH of PRO cell lysosomes basically recovered within 60 min, the pH recovery of SEN cell lysosomes appeared markedly slower (Fig. 2G). Interestingly, upon SIRT1 depletion from these cells, a similar tendency of lysosomal pH increase and post-stress pH recovery deficiency was observed, which largely resembled that of SEN cells (Fig. 2F-G).

As the data suggested defective proton pump in SEN cells, we analyzed V-ATPases, a set of multi-subunit enzymes functionally supporting the acidification of late endosomes and lysosomes (45). Immunoblots showed that expression of subunit A of V1 (ATP6V1A) substantially decreased upon cellular senescence, in parallel with SIRT1 reduction and pan-ubiquitination (Fig. 2H). Further analysis showed enhanced ubiquitination when ATP6V1A was eliminated, even with SIRT1 level unaffected, suggesting ATP6V1A is responsible for controlling protein ubiquitination, a process downstream of SIRT1 regulation (Fig. 2I). While SIRT1 elimination remarkably enhanced ubiquitination, ectopic expression of ATP6V1A was able to rescue such an effect (Fig. 2J). We then assessed the capacity of sEV secretion, and found ATP6V1A knockdown caused a significant increase in the number of sEVs released from stromal cells, an effect that largely resembled that of SIRT1 depletion (Fig. 2K). To the contrary, overexpression of either SIRT1 or ATP6V1A prominently restrained sEV production in SEN cells, although no changes were observed in PRO cells (Fig. 2L). Thus, our data consistently demonstrated that SIRT1 loss causes lysosomal de-acidification and is responsible for sEV overproduction via ATP6V1A downregulation in SEN cells, a mechanism reported for certain cancer cell types (33).

Senescent stromal sEVs enhance the malignancy of recipient cancer cells particularly therapeutic resistance

We next asked whether sEVs secreted by SEN stromal cells can exert profound impacts on cancer cells. We generated a stable PSC27 subline (PSC27-CD63) with a construct (pCT-CD63-eGFP), permitting to utilize the eGFP-fusion CD63 to mark cellular compartment, organelles and structures to enable long term and in-depth tracing of sEV biosynthesis, secretion, and uptake. Upon collection of PSC27-derived sEVs, we applied them directly to treat prostate cancer (PCa)

cells in culture (Fig. 3A). Not surprisingly, eGFP-marked CD63 was easily detected, although mainly in the perinuclear region of PCa cells, suggesting active uptake of these vesicles by recipient cancer cells (Fig. 3B).

Subsequent *in vitro* assays demonstrated that SEN stromal sEVs can significantly enhance the proliferation of several PCa cell lines including PC3, DU145, LNCaP and M12, in contrast to sEVs released from PRO stromal cells, which though also generated detectable effects (Fig. 3C). We further observed markedly increased migration and invasion of these cells upon exposure to SEN stromal sEVs (Supplementary Fig. S3A-B). More importantly, PCa cells showed significantly enhanced resistance to mitoxantrone (MIT), a type II topoisomerase inhibitor administered to treat several types of malignancies including PCa in clinical medicine (Fig. 3D). Although PRO stromal sEVs did not confer significant benefits on the survival of the majority of PCa cell lines we assayed, SEN stromal sEVs pronouncedly enhanced the resistance of cancer cells to MIT-induced cytotoxicity (Fig. 3D). We further assessed the influence of stromal sEVs on cancer cell survival with MIT, which was specifically prepared in a range of doses (0.01 ~ >1.0 μ M) designed to resemble its serum concentrations in clinical conditions. The data suggested that PRO stromal sEVs did not significantly change PC3 survival when cells were exposed to MIT, whereas SEN stromal sEVs did (Fig. 3E). We noticed that the two groups of stromal sEVs differed most dramatically in the range of 0.1-1.0 μ M MIT, although further augment of drug concentration consistently resulted in rapid clearance of cancer cells presumably due to cell intolerance against overwhelming cytotoxicity.

Mechanistic dissection revealed that MIT induced cleavage of caspase 3 in cancer cells, a process that was modestly affected by PRO stromal sEVs but remarkably weakened by SEN stromal sEVs (Fig. 3F). Although alternative cell survival pathways may be operative, our data

suggest that SEN stromal sEVs drive cancer resistance likely via a caspase-counteracting mechanism. We further applied QVD-OPH and ZVAD-FMK, two potent pan-caspase inhibitors, as well as PAC1 and gambogic acid (GA), two typical caspase activators, to individually treat PC3 cells shortly before MIT exposure. Cell apoptosis was substantially attenuated in the presence of QVD-OPH or ZVAD-FMK ($P < 0.001$) (Fig. 3G). However, once the procaspase-activating compound PAC1 or GA was used, apoptosis index was markedly elevated, thus offsetting the anti-apoptosis effect of SEN stromal sEVs ($P < 0.01$). The data were largely reproduced when docetaxel (DOC), another chemotherapeutic drug that interferes with microtubule depolymerization, was applied to the system (Supplementary Fig. S3C-D). Thus, our results consistently demonstrate that SEN stromal sEVs restrains caspase-dependent apoptosis of cancer cells, a process that underlies its resistance-boosting capacity via nanoparticle secretion-based paracrine influence on cells exposed to cytotoxic agents.

Expression profiling of prostate cancer cells is subject to profound alteration by senescent stromal sEVs

Given the remarkable changes of PCa cell phenotypes induced by senescent stromal sEVs, we next sought to determine their influence on the expression pattern of cancer cells. We first chose to perform RNA-seq to quantitate gene expression modifications and profile the transcriptomics after treatment of PCa cells with SEN stromal sEVs. Bioinformatics output showed that 344 transcripts were upregulated or downregulated significantly (≥ 2 -fold, $P < 0.05$) in PC3 cells (Supplementary Fig. S4A-B), while the expression of 422 transcripts was modified in SEN stromal sEV-affected DU145 cells (Supplementary Fig. S4C-D). Among the upregulated gene products, many are correlated with tumor development, such as CEACAM5, KRT15, IFI6, KIF20A, CEMIP and SERPINB3 in PC3, or DHRS2, IL21R, FGFBP1, DKK1, PRSS2 and

KLK6 in DU145 (Supplementary Fig. S4E-F). We noticed that these proteins are mostly involved in key biological processes such as signal transduction, cell communication, cell metabolism, energy pathways, cell growth and maintenance (Supplementary Fig. S4G-H). Therefore, data from bioinformatics analysis generally support the findings derived from *in vitro* assays, which showed enhanced cell proliferation, migration and invasiveness activities of cancer cells upon exposure to SEN stromal sEVs (Fig. 3C and Supplementary Fig. S3A-B).

Next, we performed comparative assessment by scrutinizing genes whose expression was co-upregulated in both PC3 and DU145 cells (≥ 2 -fold, $P < 0.05$). The data presented 22 genes that fell in this category, with 199 and 169 genes being uniquely upregulated in PC3 and DU145, respectively (Supplementary Fig. S4I). Interestingly, we noticed the ATP binding cassette subfamily B member 4 (ABCB4), a full transporter and member of the p-glycoprotein family of membrane proteins with phosphatidylcholine as its substrate, showed up at the top of the PC3-DU145 co-upregulated gene list (Supplementary Fig. S4J). GO analysis indicated that ABCB4 is involved in multiple activities including glycoside transport, carbohydrate export, response to drug, fenofibrate, external biotic stimulus and cellular hyperosmotic salinity (Supplementary Fig. S4K). Alternatively, KEGG appraisal underscored its biological implications as a typical ABC transporter (Supplementary Fig. S4L).

After mapping ABCB4-involved protein-protein interaction (PPI) curated with the STRING database interactome (46), we generated a network highlighting the interaction of ABCB4 with a handful of proteins such as PPARA, FABP1, CREBBP, CHD9 and CARM1 in human cells (Supplementary Fig. S4M). The PPI network encompassed protein target nodes ($n = 11$) connected by edges ($n = 55$) with an average node degree of 10 (local clustering coefficient of 1, PPI enrichment $P < 1.0e-16$). We calculated the evidence based on GO and other databases

including KEGG, PFAM and InterPro, with binary human PPI data and enrichment results validated (Supplementary Table S3).

Senescent stromal sEVs promote therapeutic resistance by upregulating ABCB4 expression in recipient cancer cells

Given the substantial impact of SEN stromal sEVs on transcriptome-wide expression of recipient cancer cells, we sought to explore the mechanism(s) supporting stromal sEV-enhanced malignancies particularly drug resistance of PCa cells. RNA-seq data showed that upon treatment with SEN stromal sEVs, PC3 and DU145 cells exhibited significantly ($P < 0.05$ for both lines) upregulated expression of ABCB4, while other members of the ABCB subfamily remained largely unchanged (Fig. 4A-B). Subsequent transcript assays essentially supported these results (Fig. 4C-D). We further confirmed the SEN stromal sEV-inducible pattern of ABCB4 by immunoblots (Fig. 4E).

Next, to address the relevance of ABCB4 upregulation to cancer cells, we eliminated this multidrug resistance protein of an ATPase-associated function responsible for drug efflux with gene-specific shRNAs (Supplementary Fig. S5A). Of note, the gain of function in cell proliferative rate after exposure to SEN stromal sEVs was largely diminished upon depletion of ABCB4 from representative PCa cell lines (Fig. 4F). We observed significantly weakened migration and invasion when ABCB4 was eliminated from these cells (Supplementary Fig. S5B-C). The effects caused by ABCB4 removal from cancer cells were further observed in chemoresistance assays, which showed a similar tendency among the PCa cell lines examined at their individual MIT concentration of IC50 (Fig. 4G-H). To expand, we further examined cell survival capacity across a wide window of MIT concentrations with PC3, and found ABCB4

knockdown caused a remarkable reduction in cell survival upon treatment by MIT in the range of 0.1 ~ 1.0 μ M (Fig. 4I). Thus, our data consistently support the key function of ABCB4 in mediating resistance to a chemotherapeutic agent, a property acquired upon uptake of SEN stromal sEVs by cancer cells.

To validate the generality of these findings, we collected sEVs from HBF1203, the breast stromal cell line, which enters cellular senescence upon DOX treatment (Supplementary Fig. S1E-H). Following a similar procedure, we eliminated ABCB4 from MDA-MB-231, a breast cancer cell line, before exposure to SEN stromal sEVs. The data from breast stroma-cancer assessments closely resembled those derived from prostate stroma-cancer assays, by showing the effect of ABCB4 depletion on BCa cell survival in a DOX concentration range of 0.1 ~ 10 μ M which approaches its plasma level of BCa patients in clinics (47) (Fig. 4J).

Activating SIRT1 restrains sEV production by senescent cells and promotes anticancer efficacy

Since SIRT1 expression is reduced in SEN stromal cells, a process responsible for increased sEV production, we reasoned the possibility of minimizing sEV production by SEN stromal cells through targeting SIRT1. To this end, we chose SRT2104 and SRT1720, two potent selective activators of SIRT1, to treat stromal cells. Simultaneous exposure of PSC27 cells to BLEO and either SIRT1 activator significantly decreased the number of sEVs released by SEN PSC27 cells (Fig. 5A and Supplementary Fig. S6A). SIRT1 activation caused remarkable deacetylation of HSF1 in SEN cells, a transcription factor that is functionally involved in proteostasis upon cellular stress via SIRT1-mediated deacetylation, paralleled by upregulation of its target HSP70 which reversely correlates with sEV production (Supplementary Fig. S2B, C and H) (48). More

importantly, we observed markedly declined ABCB4 expression and diminished chemotherapeutic resistance of PCa cells (PC3 as a representative) upon incubation with sEVs secreted by SEN stromal cells which were simultaneously exposed to BLEO-delivered genotoxicity and a SIRT1 activator (SEN/SRT2104 or SEN/SRT1720), in contrast to the senescence-naïve group (SEN or SEN/DMSO) (Supplementary Fig. S6B and Fig. 5B). The data derived from PSC27 and PC3 were largely reproducible by a similar set of assays performed with HBF1203 and MDA-MB-231, both lines of human breast origin (Supplementary Fig. S6C-D). Thus, targeting SIRT1 with pharmacological activators can restrain sEV production, a treatment strategy that is effective in governing the phenotype of SEN stromal cells but indeed correlated with significantly weakened drug resistance of cancer cells.

Given the prominent efficacy of SIRT1 activator-mediated control of sEV production by SEN stromal cells, we asked whether the *in vitro* findings can be technically repeated by *in vivo* studies. To precisely address tumor-stroma interactions in a TME context with structural and functional integrity, we generated tissue recombinants by admixing PSC27 with PC3 at a pre-optimized ratio before subcutaneously injecting them to the hind flank of experimental mice with severe combined immunodeficiency (SCID). Prior to agent-mediated therapeutics, target-specific genetic assays were performed. We noticed that expression of ectopic SIRT1 can substantially restrain sEV secretion from SEN stromal cells, largely resembling effects observed upon SIRT1 activation (Supplementary Fig. S6E). *In vivo* data indicated that the presence of stromal cells markedly increased tumor volumes (52.6%, $P < 0.001$) (Supplementary Fig. S6F). In contrast to PRO stromal cells, SEN stromal cells further promoted tumor growth (45.2%, $P < 0.001$), a tendency that was essentially abolished upon SIRT1 overexpression in PSC27 (36.4%, $P < 0.001$) (Supplementary Fig. S6F). We then initiated preclinical trials with therapeutic agents.

MIT and SRT2104 (chosen for preclinical studies due to its slightly higher efficacy than SRT1720; SRT2104 currently in phase 2 trials, while SRT1720 failed) were administered as mono or dual agents starting from the 3rd week post tumor implantation, after which animals received treatment in a metronomic manner to mimic clinical conditions (Fig. 5C and Supplementary Fig. S6G). Data from endpoint measurement of tumor size indicated that MIT administration caused remarkably delayed tumor growth, validating the efficacy of MIT as a cytotoxic agent (41.3%, $P < 0.001$) (Fig. 5D). Although treatment with SRT2104 did not significantly change tumor volume, co-administration of MIT and SRT2104 caused maximal reduction of tumor mass (63.9% shrinkage in contrast to SRT2104, or 44.0% decrease in relative to MIT given in the mono-treatment) (Fig. 5D). We observed substantially enhanced cellular senescence in tumors dissected from animals that underwent therapeutic regimens involving MIT, regardless of SRT2104 administration (Fig. 5E). Resembling the profiles captured with cultured cells, genotoxic treatment caused remarkable expansion of stromal cell MVBs which displayed augment in both size and enclosed vesicle number, a tendency restrained upon SRT2104 administration (Supplementary Fig. S6H).

Treatment-induced cellular senescence was accompanied by in-tissue development of the SASP, as evidenced by increased expression of SASP hallmark factors such as IL6, IL8, IL1 α , MMP3 (Supplementary Fig. S6I). Although stromal cells exhibited consistently increased SASP expression, cancer epithelial cells did not show a typical senescence profile, including expression of p16 which remained largely unchanged after treatment (Supplementary Fig. S6I). This was likely due to the emergence of treatment-resistant cancer cells and expansion of resistance colonies during the chemotherapeutic regimen, a process responsible for tumor relapse posttreatment. Importantly, we observed significantly decreased signals of SIRT1 in stromal

cells post-treatment, which was in line with our *in vitro* data (Fig. 2A-C). Reduction of SIRT1 in stroma was accompanied by consistently enhanced expression of sEV markers including TSG101, Syntenin-1, CD9, CD63 and CD81 (Fig. 5F). In contrast, cancer cells did not seem to develop such a distinct pattern.

Loss of SIRT1 expression was also revealed by immunohistochemistry (IHC) staining of mouse tissues. In contrast to stromal cells which showed a generally declining tendency, adjacent cancer cells appeared largely unchanged in SIRT1 expression (Fig. 5G). The data suggested the presence of a differential expression mechanism that demarcates stromal cells from their cancer epithelial counterparts. IF staining of tissues indicated that there was a remarkable increase of ABCB4 in cancer cells, but not stromal cells, after exposure of animals to MIT, although the signals were minimized when SRT2104 was delivered alongside MIT (Supplementary Fig. S6J-K).

As sEVs can foster pre-metastatic niche formation and mediate distant metastasis of cancer cells, we interrogated whether there are metastatic events in these animals. Bioluminescence imaging (BLI) of xenografts generated with PC3 cells stably expressing luciferase (PC3-luc) and PSC27 stromal cells excluded activities of cancer cell dissemination from the primary sites, while the relative BLI signal intensities essentially supported tumor growth patterns observed in xenografted mice (Fig. 5H). The data suggest that classic chemotherapy combined with a SIRT1-activating agent can achieve tumor regression more effectively than chemotherapy alone, a therapeutic strategy that holds a prominent potential to circumvent the SEN stroma-induced pathological exacerbation, specifically acquired resistance.

As a Topoisomerase II inhibitor, MIT induces apoptosis or premature senescence in the TME niche, depending on the cell type and agent dose (49,50). Tissue assessment indicated that MIT administration to these animals caused dramatically increased DNA damage and apoptosis in cancer epithelial cells, as evidenced by DDR foci measurement and caspase 3 cleavage appraisal (Fig. 5I). In starking contrast, stromal cells manifested development of DDR foci, limited apoptosis, but markedly enhanced senescence, indicating a response and cell fate distinct from their adjacent cancer counterparts after exposure to MIT-delivered cytotoxicity (Fig. 5I; Supplementary Fig. S6L). Although SRT2104 alone did not induce typical DDR or apoptosis, significantly elevated indices of both DNA damage and apoptosis were observed in tissues of animals that underwent MIT/SRT2104 combinatorial treatment. In contrast to the MIT-only group, there was a pronounced increase of DDR and apoptosis in MIT/SRT2104 animals (40.3% and 112.5%, respectively), suggesting a remarkable potential of SRT2104 in promoting cancer cell clearance and achieving tumor regression when synergized with classic chemotherapy *in vivo* (Fig. 5I-J).

SIRT1 decline in senescent stromal cells and ABCB4 expression in cancer cells predict adverse outcome post-chemotherapy

We next interrogated the pathological relevance of SIRT1 reduction in stroma and ABCB4 elevation in cancer cells to patient survival after chemotherapy. Upon IHC staining, we observed enhanced p16^{INK4a} expression in stromal cells of patients who experienced chemotherapeutic intervention, while most cancer cells remained largely negative (Fig. 6A). The data revealed comprehensive occurrence of cellular senescence in the stroma while cancer cells seemingly resisted in the gland, presumably through expansion from colonies that survived anticancer treatments via development of drug resistance. We noticed remarkably decreased expression of

SIRT1 in stromal, rather than their adjacent cancer cells, although the latter showed elevated ABCB4 expression in posttreatment patients (Fig. 6A).

Upon precise isolation of stromal and cancer cell subpopulations with laser capture microdissection (LCM) and evaluation by qRT-PCR, we noticed SIRT1 reduction and ABCB4 elevation in stromal and epithelial cells, respectively (Fig. 6B-C). Thus, transcript expression data were essentially consistent with those acquired from tissue staining appraisal of these clinical specimens.

We further performed a sample-based clinical investigation by randomly choosing two subgroups of PCa patients (10 for each) from the overall cohort, including one that did not undergo chemotherapy and the other that experienced chemotherapy, with patient-derived peripheral blood samples available from both subgroups. TSG101-specific ELISA tests suggested significantly enhanced levels of circulating sEVs in the serum of post-treatment patients, as compared with those untreated individuals (Fig. 6D). Surprisingly, immunoblots even showed clearly visible signals of circulating sEVs (Syntenin-1, TSG101 and ALIX-positivity) in the serum of post-treatment patients (3 out of 5 cases), in sharp contrast to samples from those untreated which were generally negative (Fig. 6E). Therefore, sEVs in the circulating system of post-treatment patients hold the potential to be evaluated as blood-borne substance for clinical monitoring via examination with routine biotechniques.

We next sought to establish the consequence of enhanced sEV biogenesis in these patients. After tissue staining against SIRT1 and ABCB4, we assessed these patients by associating the results with their survival. Strikingly, there was a significant and positive correlation between stromal SIRT1 expression and patient disease-free survival (DFS) in the post-treatment PCa

cohort (Fig. 6F). To the contrary, a significant but negative correlation was observed between cancer cell ABCB4 expression and patient survival (Fig. 6G). Thus, SIRT1 decline-mediated sEV production and release by stromal cells, combined with ABCB4 upregulation in cancer cells, can provide a novel and precise avenue for prognosis of advanced malignancies in future cancer medicine. Specifically, given the prominent relevance of SIRT1 loss in sEV biogenesis of SEN stromal cells and its hitherto well documented implications in human pathologies, we would propose SIRT1 as a functionally multifactorial target in clinical oncology.

Discussion

Mutual interaction between cancer cells and the surrounding TME is crucial for malignant progression. Numerous studies have unraveled the paracrine signaling of various cytokines, chemokines and growth factors through their receptors as a key means of intercellular communication in the TME. In contrast, EVs have recently emerged as another mechanism to mediate cell-cell interactions, which can be secreted from various cell types (51). As a subclass of EVs, sEVs contain various proteins, mRNAs, microRNAs, lipids and even DNA fragments. To date, most cancer-associated sEV studies focus on cancer cells or proliferating cells. In contrast, here we present evidence to show that senescent stromal cells, which abundantly reside in host tissues, are responsible for cancer progression by producing sEVs to shape drug resistance acquired from the treatment-damaged TME (Fig. 6H).

Sirtuins (SIRT1-7) belong to the 3rd class of HDACs, whose activities are dependent on NAD⁺ (52). In this study, we revealed SIRT1 as the most dramatically declined sirtuin molecule in senescent stromal cells. Protein quality control is critical for maintenance of cell physiology,

while damaged proteins need to be restored or degraded, a process mainly supported by molecular chaperones and the ubiquitin-proteasome system. Interestingly, both proteasome and autophagy machineries remained largely intact in these cells. SIRT1 reduction correlates with enhanced expression of multiple sEV markers and is responsible for ATP6V1A downregulation, resulting in defective lysosomal acidification and sEV overproduction. The data are reminiscent of a recent study which demonstrated that genetic or pharmacological inhibition of SIRT1 destabilizes the mRNA of ATP6V1A, leading to deficient lysosomal acidification, MVB enlargement and enhanced exosome production (33). While our observation was mainly regarding senescent stromal cells, distinct from the discovery recently made in human breast cancer cells, a similarly occurring MVB expansion suggests that senescent stromal cells somehow resemble cancer cells with regard to sEV biogenesis. Further, SIRT1 loss-driven ATP6V1A downregulation results in defective lysosomal acidification and increase of pH to approximately 6.0, partially explaining the comprehensively observed SA- β -Gal staining positivity of senescent cells, a phenomenon reported long time ago but rarely addressed for underlying mechanism(s) (53).

There is a growing interest in the discovery of small molecules modifying sirtuin activities, although most sirtuin activators have been described intensively for SIRT1 (54). Specifically, SIRT1 has been suggested to play multiple and, in some cases, contradictory roles in cancer, by functioning as either a tumor suppressor or tumor promoter, depending on tissue type and pathological context (33). *In vivo* stimulation of SIRT1 either with agonist or NAD⁺ precursors can extend the lifespan of mice and protect against diverse aging-related diseases (55). Resveratrol is a natural polyphenol compound which activates SIRT1, holding potential in treatment or prevention of tumorigenesis and aging-related diseases, but it has limited

bioavailability (56). Molecules structurally unrelated to resveratrol, including SRT1720 and SRT2104, are typically sirtuin-activating compounds (STACs) developed to stimulate sirtuin activities more potently than resveratrol, with markedly improved bioavailability (57). In our study, we disclosed that SIRT1 activators including SRT2104 can effectively restrain sEV biogenesis in senescent stromal cells. Although cancer cells exposed to the stromal CM containing sEVs developed remarkably enhanced malignancy, addition of SRT2104 to the system was able to counteract such a tendency. Alternatively, treatment with nicotinamide mononucleotide (NMN), a key precursor of NAD^+ , represents another potential option to enhance stromal cell SIRT1 activity and minimize cancer resistance, with future work warranted to demonstrate the efficacy.

Our study support that senescent stromal cells produce an increased number of sEVs, which can be conceptually considered as part of the full SASP spectrum. However, one of the limitations is the lack of a dataset showing the distinct profile of proteomic composition in senescent stromal cells, which may be exploited as a reservoir for screening novel targets. Second, other bioactive contents such as miRNAs, which specifically merit future investigation, may serve as novel prognostic markers for evaluation of treatment consequence in cancer clinics. Third, sEV size redistribution in proliferating vs senescent stromal cells deserves attention, as this potentially correlates with cargo alterations, a case awaiting future studies to disclose the relevant mechanism(s). Fourth, the impact of pan-ubiquitination on senescent cell metabolism and long term survival remains unexplored and represents an intriguing question. Despite these issues, as a special note, combination of conventional chemotherapy theoretically designed to target cancer cells, with a SIRT1 activator like SRT2104, can significantly improve therapeutic outcome by restraining sEV biogenesis in senescent stromal cells, which frequently arise as a

part of side-effects of anticancer agents and are responsible for multiple age-related pathologies including but not limited to the most lethal form, cancer.

Disclosure of Potential Conflicts of Interest

No potential conflicts of interest were disclosed.

Acknowledgements

This work was supported by grants from National Key Research and Development Program of China (2016YFC1302400 to Y. Sun), National Natural Science Foundation of China (NSFC) (81472709, 31671425, 31871380 to Y. Sun), CAS Key Laboratory of Tissue Microenvironment and Tumor of Chinese Academy of Sciences (to Y. Sun), the National 1000 Young Talents Research Program of China (to Y. Sun), Anti-Aging Collaborative Program of SIBS and BY-HEALTH (C01201911260006 to Y. Sun), the University and Locality Collaborative Development Program of Yantai (2019XDRHXMRC08 to Y. Sun), and the US Department of Defense (DoD) Prostate Cancer Research Program (PCRP) (Idea Development Award PC111703 to Y. Sun); National Science and Technology Major Project of China (2019ZX09732002-14) to J. Jiang.; CRUK (A12011), Breast Cancer Now (2012MayPR070; 2012NovPhD016), the Medical Research Council of the United Kingdom (MR/N012097/1), Imperial ECMC and NIHR Imperial BRC to E.W-F. Lam.

References

1. Karagiannis GS, Pastoriza JM, Wang YR, Harney AS, Entenberg D, Pignatelli J, *et al.* Neoadjuvant

- chemotherapy induces breast cancer metastasis through a TMEM-mediated mechanism. *Sci Transl Med* 2017;9:eaan0026.
2. Wagner AH, Devarakonda S, Skidmore ZL, Krysiak K, Ramu A, Trani L, *et al.* Recurrent WNT pathway alterations are frequent in relapsed small cell lung cancer. *Nature Communications* 2018;9.
 3. Ponde NF, Zardavas D, Piccart M. Progress in adjuvant systemic therapy for breast cancer. *Nature reviews Clinical oncology* 2019;16:27-44.
 4. Mucaki EJ, Zhao JZL, Lizotte DJ, Rogan PK. Predicting responses to platin chemotherapy agents with biochemically-inspired machine learning. *Signal Transduction and Targeted Therapy* 2019;4:1-12.
 5. Shaked Y. Balancing efficacy of and host immune responses to cancer therapy: the yin and yang effects. *Nature reviews Clinical oncology* 2016;13:611-26.
 6. Cooper J, Giancotti FG. Integrin Signaling in Cancer: Mechanotransduction, Stemness, Epithelial Plasticity, and Therapeutic Resistance. *Cancer cell* 2019;35:347-67.
 7. Sun Y, Coppe JP, Lam EW. Cellular Senescence: The Sought or the Unwanted? *Trends Mol Med* 2018;24:871-85.
 8. Storer M, Mas A, Robert-Moreno A, Pecoraro M, Ortells MC, Di Giacomo V, *et al.* Senescence is a developmental mechanism that contributes to embryonic growth and patterning. *Cell* 2013;155:1119-30.
 9. Munoz-Espin D, Canamero M, Maraver A, Gomez-Lopez G, Contreras J, Murillo-Cuesta S, *et al.* Programmed cell senescence during mammalian embryonic development. *Cell* 2013;155:1104-18.
 10. Demaria M, Ohtani N, Youssef SA, Rodier F, Toussaint W, Mitchell JR, *et al.* An essential role for senescent cells in optimal wound healing through secretion of PDGF-AA. *Developmental cell* 2014;31:722-33.
 11. Demaria M, O'Leary MN, Chang J, Shao L, Liu S, Alimirah F, *et al.* Cellular Senescence Promotes Adverse Effects of Chemotherapy and Cancer Relapse. *Cancer discovery* 2017;7:165-76.
 12. Hernandez-Segura A, Nehme J, Demaria M. Hallmarks of Cellular Senescence. *Trends in cell biology* 2018;28:436-53.
 13. Coppe JP, Patil CK, Rodier F, Sun Y, Munoz DP, Goldstein J, *et al.* Senescence-associated secretory phenotypes reveal cell-nonautonomous functions of oncogenic RAS and the p53 tumor suppressor. *PLoS biology* 2008;6:2853-68.
 14. Kuilman T, Michaloglou C, Vredeveld LCW, Douma S, van Doom R, Desmet CJ, *et al.* Oncogene-induced senescence relayed by an interleukin-dependent inflammatory network. *Cell* 2008;133:1019-31.
 15. Acosta JC, O'Loughlen A, Banito A, Guijarro MV, Augert A, Raguz S, *et al.* Chemokine signaling via the CXCR2 receptor reinforces senescence. *Cell* 2008;133:1006-18.
 16. Lee S, Schmitt CA. The dynamic nature of senescence in cancer. *Nat Cell Biol* 2019;21:94-101.
 17. Tasdemir N, Banito A, Roe JS, Alonso-Curbelo D, Camiolo M, Tschaharganeh DF, *et al.* BRD4 Connects Enhancer Remodeling to Senescence Immune Surveillance. *Cancer discovery* 2016;6:612-29.
 18. Shah PP, Donahue G, Otte GL, Capell BC, Nelson DM, Cao K, *et al.* Lamin B1 depletion in senescent cells triggers large-scale changes in gene expression and the chromatin landscape. *Genes Dev* 2013;27:1787-99.
 19. Dou Z, Xu C, Donahue G, Shimi T, Pan JA, Zhu J, *et al.* Autophagy mediates degradation of nuclear lamina. *Nature* 2015;527:105-9.
 20. Dou ZX, Ghosh K, Vizioli MG, Zhu JJ, Sen P, Wangenstein KJ, *et al.* Cytoplasmic chromatin triggers inflammation in senescence and cancer. *Nature* 2017;550:402-6.
 21. Gluck S, Guey B, Gulen MF, Wolter K, Kang TW, Schmacke NA, *et al.* Innate immune sensing of cytosolic chromatin fragments through cGAS promotes senescence. *Nat Cell Biol* 2017;19:1061-70.
 22. Pathan M, Fonseka P, Chitti SV, Kang T, Sanwlani R, Van Deun J, *et al.* Vesiclepedia 2019: a compendium of RNA, proteins, lipids and metabolites in extracellular vesicles. *Nucleic Acids Res* 2019;47:D516-D9.
 23. Tkach M, Thery C. Communication by Extracellular Vesicles: Where We Are and Where We Need to Go. *Cell* 2016;164:1226-32.
 24. Han L, Xu J, Xu Q, Zhang B, Lam EW, Sun Y. Extracellular vesicles in the tumor microenvironment: Therapeutic resistance, clinical biomarkers, and targeting strategies. *Medicinal research reviews* 2017;37:1318-49.
 25. Sun Y, Campisi J, Higano C, Beer TM, Porter P, Coleman I, *et al.* Treatment-induced damage to the tumor microenvironment promotes prostate cancer therapy resistance through WNT16B. *Nat Med* 2012;18:1359-68.
 26. Zhang BY, Fu D, Xu QX, Cong XL, Wu CY, Zhong XM, *et al.* The senescence-associated secretory phenotype

- is potentiated by feedforward regulatory mechanisms involving Zscan4 and TAK1. *Nat Commun* 2018;9:1723.
27. Xu Q, Long Q, Zhu D, Fu D, Zhang B, Han L, *et al.* Targeting amphiregulin (AREG) derived from senescent stromal cells diminishes cancer resistance and averts programmed cell death 1 ligand (PD-L1)-mediated immunosuppression. *Aging cell* 2019;18:e13027.
 28. Mathieu M, Martin-Jaular L, Lavieu G, Thery C. Specificities of secretion and uptake of exosomes and other extracellular vesicles for cell-to-cell communication. *Nat Cell Biol* 2019;21:9-17.
 29. Thery C, Witwer KW, Aikawa E, Alcaraz MJ, Anderson JD, Andriantsitohaina R, *et al.* Minimal information for studies of extracellular vesicles 2018 (MISEV2018): a position statement of the International Society for Extracellular Vesicles and update of the MISEV2014 guidelines. *J Extracell Vesicles* 2018;7:1535750.
 30. Menck K, Sonmezer C, Worst TS, Schulz M, Dihazi GH, Streit F, *et al.* Neutral sphingomyelinases control extracellular vesicles budding from the plasma membrane. *J Extracell Vesicles* 2017;6:1378056.
 31. Miao Y, Li G, Zhang X, Xu H, Abraham SN. A TRP Channel Senses Lysosome Neutralization by Pathogens to Trigger Their Expulsion. *Cell* 2015;161:1306-19.
 32. Villarrojo-Beltri C, Baixauli F, Mittelbrunn M, Fernandez-Delgado I, Torralba D, Moreno-Gonzalo O, *et al.* ISGylation controls exosome secretion by promoting lysosomal degradation of MVB proteins. *Nat Commun* 2016;7:13588.
 33. Latifkar A, Ling L, Hingorani A, Johansen E, Clement A, Zhang X, *et al.* Loss of Sirtuin 1 Alters the Secretome of Breast Cancer Cells by Impairing Lysosomal Integrity. *Developmental cell* 2019;49:393-408 e7.
 34. Eren MK, Kilincli A, Eren O. Resveratrol Induced Premature Senescence Is Associated with DNA Damage Mediated SIRT1 and SIRT2 Down-Regulation. *PLoS one* 2015;10.
 35. Sasaki T, Maier B, Bartke A, Scoble H. Progressive loss of SIRT1 with cell cycle withdrawal. *Aging cell* 2006;5:413-22.
 36. Anwar T, Khosla S, Ramakrishna G. Increased expression of SIRT2 is a novel marker of cellular senescence and is dependent on wild type p53 status. *Cell cycle* 2016;15:1883-97.
 37. Tomita T, Hamazaki J, Hirayama S, McBurney MW, Yashiroda H, Murata S. Sirt1-deficiency causes defective protein quality control. *Scientific reports* 2015;5:12613.
 38. Chien Y, Scuoppo C, Wang X, Fang X, Balgley B, Bolden JE, *et al.* Control of the senescence-associated secretory phenotype by NF-kappaB promotes senescence and enhances chemosensitivity. *Genes Dev* 2011;25:2125-36.
 39. Chen F, Long Q, Fu D, Zhu D, Ji Y, Han L, *et al.* Targeting SPINK1 in the damaged tumour microenvironment alleviates therapeutic resistance. *Nat Commun* 2018;9:4315.
 40. Yamakuchi M, Ferlito M, Lowenstein CJ. miR-34a repression of SIRT1 regulates apoptosis. *Proceedings of the National Academy of Sciences of the United States of America* 2008;105:13421-6.
 41. Nassour J, Martien B, Martin N, Deruy E, Tomellini E, Malaquin N, *et al.* Defective DNA single-strand break repair is responsible for senescence and neoplastic escape of epithelial cells. *Nature Communications* 2016;7.
 42. Siong Tan HW, Anjum B, Shen HM, Ghosh S, Yen PM, Sinha RA. Lysosomal inhibition attenuates peroxisomal gene transcription via suppression of PPARA and PPARGC1A levels. *Autophagy* 2019;1-5.
 43. Zhang H, Han B, Lu H, Zhao Y, Chen X, Meng Q, *et al.* USP22 promotes resistance to EGFR-TKIs by preventing ubiquitination-mediated EGFR degradation in EGFR-mutant lung adenocarcinoma. *Cancer Lett* 2018;433:186-98.
 44. Buter J, Cheng TY, Ghanem M, Grootemaat AE, Raman S, Feng XX, *et al.* Mycobacterium tuberculosis releases an antacid that remodels phagosomes. *Nat Chem Biol* 2019;15:889-+.
 45. Chung CY, Shin HR, Berdan CA, Ford B, Ward CC, Olzmann JA, *et al.* Covalent targeting of the vacuolar H(+)-ATPase activates autophagy via mTORC1 inhibition. *Nat Chem Biol* 2019;15:776-85.
 46. Szklarczyk D, Morris JH, Cook H, Kuhn M, Wyder S, Simonovic M, *et al.* The STRING database in 2017: quality-controlled protein-protein association networks, made broadly accessible. *Nucleic Acids Res* 2017;45:D362-D8.
 47. Chekin F, Myshin V, Ye R, Melinte S, Singh SK, Kurungot S, *et al.* Graphene-modified electrodes for sensing doxorubicin hydrochloride in human plasma. *Anal Bioanal Chem* 2019;411:1509-16.
 48. Brunquell J, Raynes R, Bowers P, Morris S, Snyder A, Lugano D, *et al.* CCAR-1 is a negative regulator of the heat-shock response in *Caenorhabditis elegans*. *Aging cell* 2018;17:e12813.

49. Liu Q, Chen F, Hou L, Shen L, Zhang X, Wang D, *et al.* Nanocarrier-Mediated Chemo-Immunotherapy Arrested Cancer Progression and Induced Tumor Dormancy in Desmoplastic Melanoma. *Acs Nano* 2018;12:7812-25.
50. Laberge RM, Sun Y, Orjalo AV, Patil CK, Freund A, Zhou L, *et al.* MTOR regulates the pro-tumorigenic senescence-associated secretory phenotype by promoting IL1A translation. *Nat Cell Biol* 2015;17:1049-61.
51. Kalluri R. The biology and function of exosomes in cancer. *J Clin Invest* 2016;126:1208-15.
52. Chalkiadaki A, Guarente L. The multifaceted functions of sirtuins in cancer. *Nature reviews Cancer* 2015;15:608-24.
53. Dimri GP, Lee XH, Basile G, Acosta M, Scott C, Roskelley C, *et al.* A Biomarker That Identifies Senescent Human-Cells in Culture and in Aging Skin in-Vivo. *Proceedings of the National Academy of Sciences of the United States of America* 1995;92:9363-7.
54. Bonkowski MS, Sinclair DA. Slowing ageing by design: the rise of NAD(+) and sirtuin-activating compounds. *Nat Rev Mol Cell Biol* 2016;17:679-90.
55. Zainabadi K. Drugs targeting SIRT1, a new generation of therapeutics for osteoporosis and other bone related disorders? *Pharmacol Res* 2019;143:97-105.
56. Villalba JM, Alcain FJ. Sirtuin activators and inhibitors. *Biofactors* 2012;38:349-59.
57. Nassir F, Ibdah JA. Sirtuins and nonalcoholic fatty liver disease. *World journal of gastroenterology : WJG* 2016;22:10084-92.

Figure Legends

Figure 1. Stromal cells produce an increased number of sEVs with distinct size distribution upon senescence. (A) Quantitative comparison of the number of sEVs secreted from proliferating (PRO) and senescent (SEN) PSC27 cells in 3 consecutive days and detected by NTA. Bleomycin (BLEO) was used to induce senescence. (B) Concentration (mean \pm SD; n = 5 acquisitions of one sample per condition) and size distribution of sEVs calculated by NTA. Left, PRO; Right, SEN. (C) Average diameter of sEVs secreted by PRO and SEN cells. Data from NTA assessment. (D) Representative transmission electron microscopy (TEM) images of sEVs isolated from stromal cells (n = 3 independent biological samples). Scale bars, 100 nm. (E) Coomassie brilliant blue stained SDS-PAGE gel showing visible difference at multiple sizes (red stars) between PRO and SEN stromal cell sEVs. Lysates loaded upon normalization to the number of sEVs. (F) Coomassie brilliant blue stained protein gel, with sEV lysates loaded upon normalization to the number of parental cells. Red line, the range of proteins that show remarkable difference. (G) Immunoblot analysis of stromal cell-derived total sEVs

collected in 3 days, with the lysate loading normalized to parental cell number. **(H)** Immunoblot analysis of whole lysates of parental cells. **(I)** Immunofluorescence staining of PRO and SEN stromal cells with CD63 and TSG101. Scale bars, 10 μ m. Arrows, sEVs in synthesis (TSG101 positive). **(J)** TEM of stromal cells, with the representative images showing multivesicular bodies (MVBs) in PRO and SEN cells, respectively. Scale bars, 300 nm. **(K)** Comparative statistics of the diameter of MVBs in PRO vs SEN stromal cells, with MVBs representative of each cell state (27 cells/group). **(L)** Quantitative expression assay of sEV biomarker and biogenesis-related molecules, with SASP hallmark factors assessed in parallel. **(M)** NTA measurement of the number of P100-EVs (sEVs) and P14-EVs (MVs) released from stromal cells, after successive differential ultracentrifugation, with the data normalized to cell number per vehicle subtype. \wedge , $P > 0.05$; *, $P < 0.05$; **, $P < 0.01$; ***, $P < 0.001$.

Figure 2. SIRT1 loss mediates lysosomal de-acidification and sEV overproduction through ATP6V1A downregulation. **(A)** Heatmap displaying the expression patterns of human SIRT family members (1-7) in PSC27 cells after senescence. Bleomycin (BLEO) was used to induce cellular senescence. Data derived from RNA-seq. **(B)** Quantitative expression assessment of SIRTs at transcription level in SEN stromal cells by qRT-PCR assays. **(C)** Immunoblot analysis of SIRT1 and the SASP hallmark factors IL8/MMP3 expression in SEN cells induced by BLEO treatment. **(D)** Transcript analysis of sEV-associated biomarkers upon shRNA-mediated knockdown of SIRT1 in PSC27 cells. **(E)** Stromal cells were subject to treatment by NAM or SRT2104 (a small molecule inhibitor and activator, respectively, of SIRT1), alone or together with BLEO, with lysates analyzed by immunoblots after 7 days. **(F)** Lysosomal pH measurements were

performed for PRO and SEN cells. Scramble (SCR) and SIRT1-specific shRNAs were transduced to stromal cells to establish stable sublines and assayed for pH, individually. (G) Percentage of re-acidification of stromal cell lysosomes posttreatment by Bafilomycin A1. Values were determined with LysoTracker Green DND-26. (H) Immunoblot examination of ATP6V1A, SIRT1 and ubiquitin levels in CTRL and BLEO cells. (I) Immunoblot analysis of ATP6V1A, SIRT1 and ubiquitin levels in stromal cells transduced with SCR or ATP6V1A-specific shRNAs. (J) Immunoblot of ATP6V1A, SIRT1 and ubiquitin in stromal cells transduced with control or SIRT1-specific shRNAs. An empty vector or ATP6V1A construct was used. (K) NTA assay of vesicle number. Stromal cells were transduced with SCR, SIRT1-specific or ATP6V1A-specific shRNAs. (L) NTA measurement of vesicle secretion. Empty vector, SIRT1 or ATP6V1A construct was transduced to cells. [^], $P > 0.05$; *, $P < 0.05$; **, $P < 0.01$; ***, $P < 0.001$.

Figure 3. Senescent stromal sEVs promote the malignant phenotypes particularly drug resistance of prostate cancer cells. (A) Schematic workflow of conditioned media (CM) collection, sequential ultracentrifugation-based sEV preparation from stromal cells and *in vitro* phenotyping of cancer cells. Bleomycin (BLEO) was used to induce senescence. (B) PSC27 cells were transduced with the pCT-CD63-eGFP construct, and the secreted sEVs were collected to treat PC3 and DU145 cells before immunofluorescence imaging. Scale bar, 20 μ m. (C) PCa cells were treated with sEVs from PSC27 cells for 3 d, and subject to proliferation assay. DMEM, blank control; PRO-sEVs, sEVs of PRO PSC27 cells; SEN-sEVs, sEVs of SEN PSC27 cells. Right, representative images. Scale bar, 40 μ m. (D) Chemoresistance assay of PCa cells cultured with stromal cell sEVs described in (C). Mitoxantrone (MIT) was applied at the

concentration of IC50 value pre-determined per cell line. Cells were cultured in DMEM, which was also used as a drug vehicle. **(E)** Dose-response curves (non-linear regression/curve fit) plotted from drug-based survival assays of PC3 cells cultured with the sEVs collected from PRO or SEN PSC27 cells, and concurrently exposed to a wide range of MIT concentrations. **(F)** Immunoblot analysis of caspase 3 cleavage in PC3 cells upon exposure to different conditions. MIT was applied at the IC50 value predetermined for PC3. **(G)** Apoptotic assay for combined activities of caspase 3/7 determined 24 h after exposure of PC3 cells to stromal cell sEVs. Cancer cells were treated by MIT with or without caspase inhibitors including QVD-OPH and ZVAD-FMK, or caspase activators including PAC1 and gambogic acid (GA). *, $P < 0.05$; **, $P < 0.01$; ***, $P < 0.001$.

Figure 4. Senescent stromal sEVs enhance drug resistance via upregulation of ABCB4 in recipient cancer cells. **(A)** Heatmap depicting the expression patterns of 11 members of human ABCB subfamily in PC3 cells upon exposure to PRO vs SEN stromal sEVs. Bleomycin (BLEO) was used to induce senescence. **(B)** Heatmap displaying the expression profiles of 11 members of the ABCB subfamily in DU145 cells upon exposure to PRO vs SEN stromal sEVs. **(C)** Quantitative RT-PCR transcript assays of the expression of human ABCB subfamily members in PC3 after incubation with sEVs for 3 consecutive days. Signals normalized to control group (DMEM). **(D)** Transcript expression assays of human ABCB subfamily member expression in DU145. **(E)** Immunoblot analysis of ABCB4 expression in PC3 and DU145 after exposure to PRO vs SEN stromal sEVs for 3 consecutive days. **(F)** Proliferation assay of PCa cells exposed to PRO vs SEN stromal sEVs for 3 days, with cancer cells depleted of ABCB4.

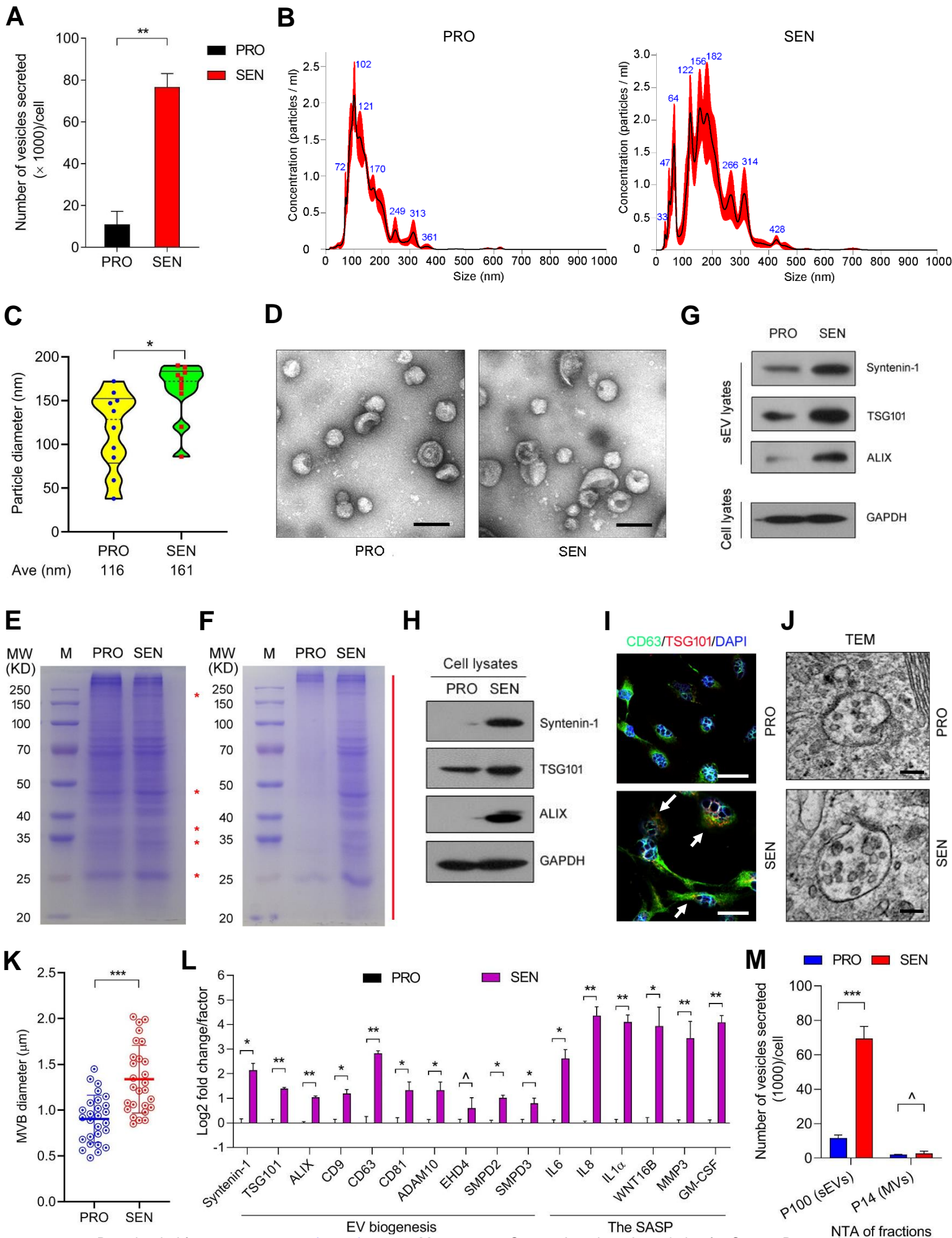
(G) Chemoresistance assay of PCa cells exposed to sEVs from PRO vs SEN stromal cells. ABCB4 eliminated in cancer cells, with MIT applied at IC50 value per cell line. (H) Representative images of PC3 examined under conditions described in G. Scale bar, 100 μ m. (I) Dose-response curves (non-linear regression/curve fit) plotted from drug-based survival assays of PC3 exposed to stromal sEVs, concurrently treated by a wide range of MIT concentrations. (J) Dose-response curves of MDA-MB-231 similar to those shown in (I), with doxorubicin (DOX)-based survival assays performed. \wedge , $P > 0.05$; *, $P < 0.05$; **, $P < 0.01$; ***, $P < 0.001$.

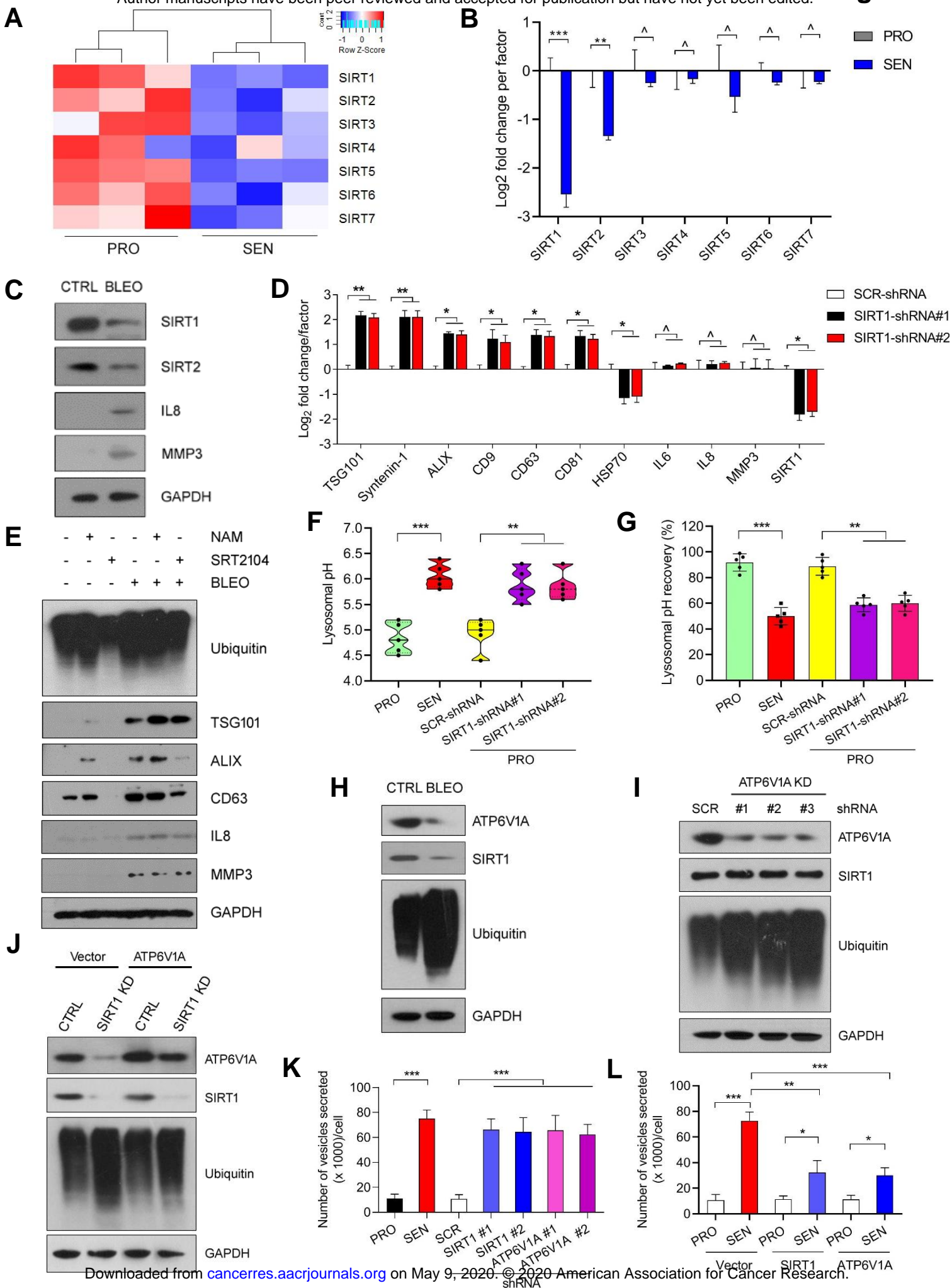
Figure 5. Targeting SIRT1 with an agonist compound to control sEV production by senescent stromal cells improves chemotherapeutic efficacy. (A) Activation of SIRT1 restrains sEV production in SEN stromal cells. SRT2104 was used to treat PSC27 alone or together with BLEO for 7-10 d. HSF1 acetylation level was evaluated via immunoprecipitation (IP, anti-HSF1) followed by immunoblot (IB, anti-AcK for acetylated lysine), with HSP70 expression assessed in parallel (GAPDH, control). (B) Dose-response curves plotted from drug-based survival assays of PC3 exposed to sEVs derived from stromal cells treated by BLEO and/or SRT2104 (or SRT1720). (C) Schematic illustration of preclinical treatments performed with immunodeficient mice. (D) Statistics of tumor end volumes. PC3 cells were xenografted together with PSC27 cells (totally 1.25×10^4 , in a cancer/stromal ratio of 4:1) to the hind flank of mice. SRT2104 and MIT were administered alone or together to induce tumor regression. (E) Representative images of *in vivo* cellular senescence after SRT2104- and/or MIT-mediated treatment. Scale bar, 100 μ m. (F) Transcript assay of sEV biomarkers expressed in epithelial and stromal cells isolated from tumors via LCM. (G)

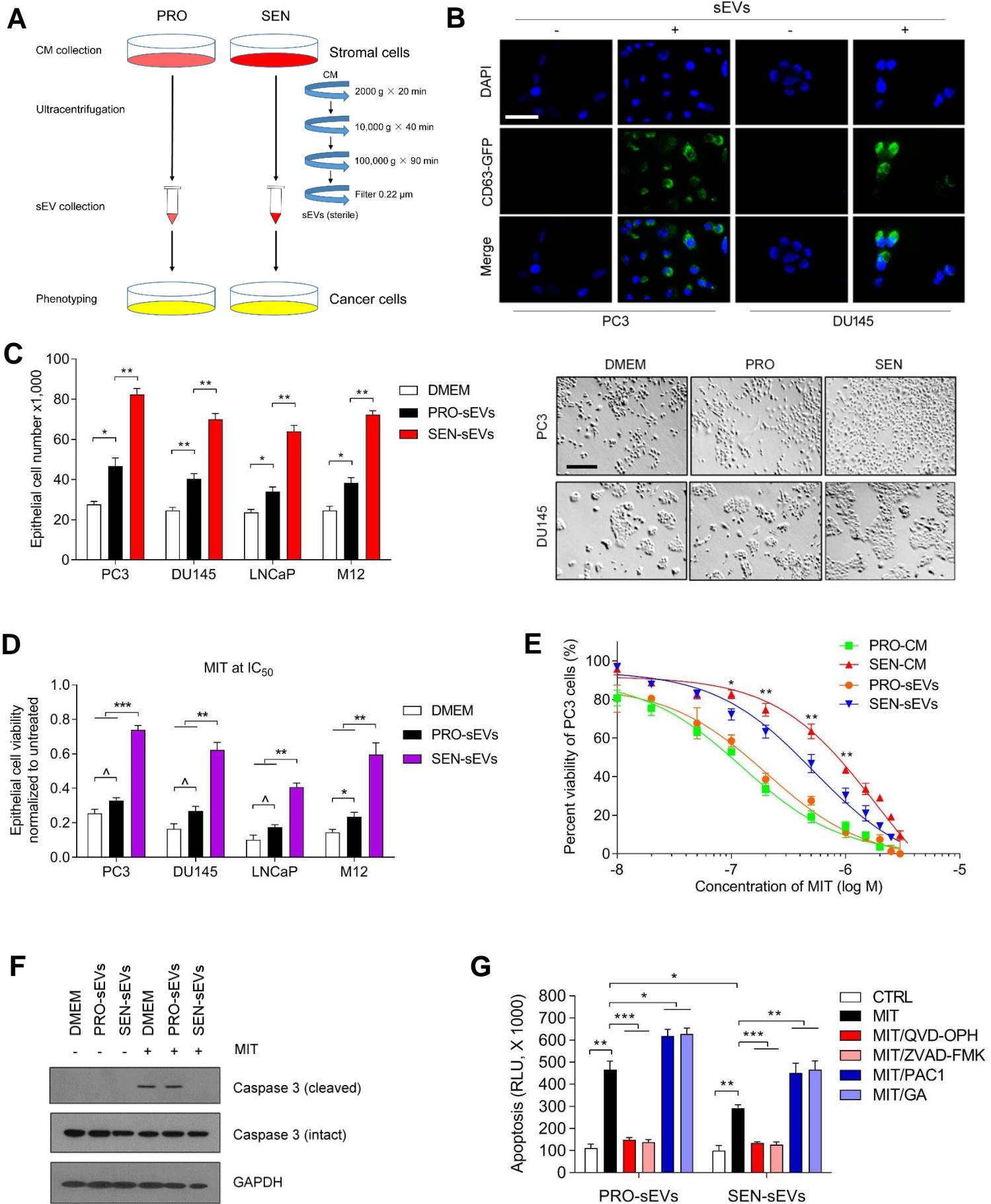
Representative IHC images of SIRT1 expression in tissues isolated from placebo or MIT-treated animals. Scale bar, 200 μ m. **(H)** Representative bioluminescence images (BLI) of PC3/PSC27 tumor-bearing animals in the preclinical trial. **(I)** Statistical evaluation of DNA-damaged and apoptotic cells in the biospecimens. Values are presented as percentage of cells positively stained by immunofluorescence staining with antibodies against γ -H2AX or caspase 3 (cleaved), individually (Vimentin/E-cadherin probed to identify stromal/epithelial cells, respectively). **(J)** Representative IHC images of caspase 3 (cleaved) in tumors at the end of therapeutic regimes. Scale bar, 200 μ m. \wedge , $P > 0.05$; *, $P < 0.05$; **, $P < 0.01$; ***, $P < 0.001$.

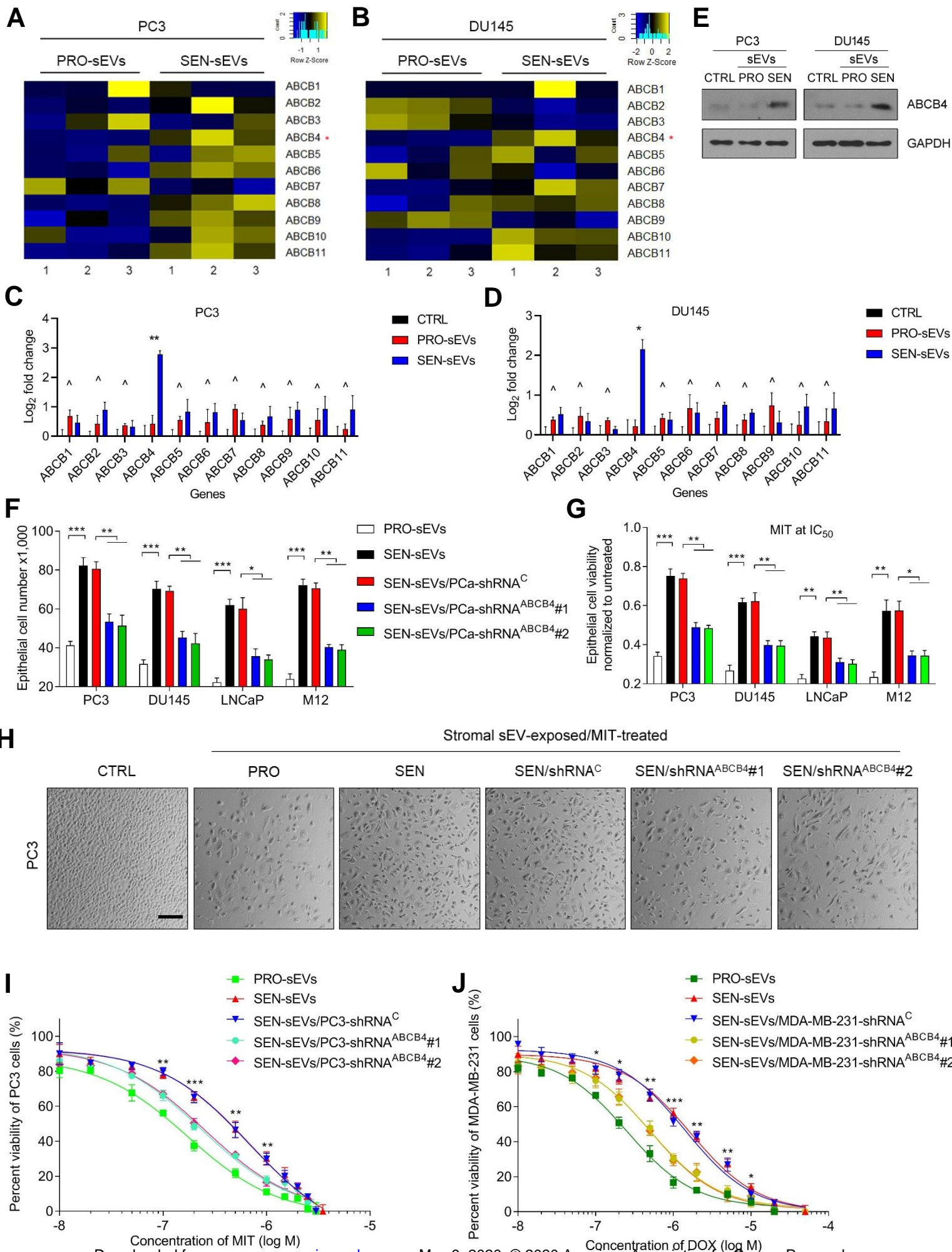
Figure 6. SIRT1 loss in stroma and ABCB4 upregulation in cancer cells predict adverse clinical outcome. **(A)** IHC assessment of human prostate tumors before and after chemotherapy. From top to bottom, representative images of p16^{INK4a}, SIRT1 and ABCB4 expression. All samples from a longitudinal study of a same patient. Scale bars, 200 μ m. **(B)** Transcript expression assay of SIRT1 in stromal cells isolated via LCM from tumor samples (20 untreated and 20 chemo-treated PCa patients randomly selected). **(C)** Transcript expression assay of ABCB4 in cancer cells isolated via LCM from tumors. **(D)** Measurement of sEVs in peripheral blood of PCa patients with TSG101-specific ELISA performed among 10 patients randomly selected from each cohort. **(E)** Immunoblot of Syntenin-1, TSG101, and ALIX, a set of typical markers of sEVs, in serum of PCa patients collected before and after chemotherapy. Albumin, loading control for patient serum. **(F)** Kaplan-Meier (KM) survival of chemo-treated PCa patients stratified with SIRT1 levels in tumor stroma. **(G)** KM assay of chemo-treated PCa patients stratified with ABCB4 levels in tumor foci. **(H)** Illustrative working model of

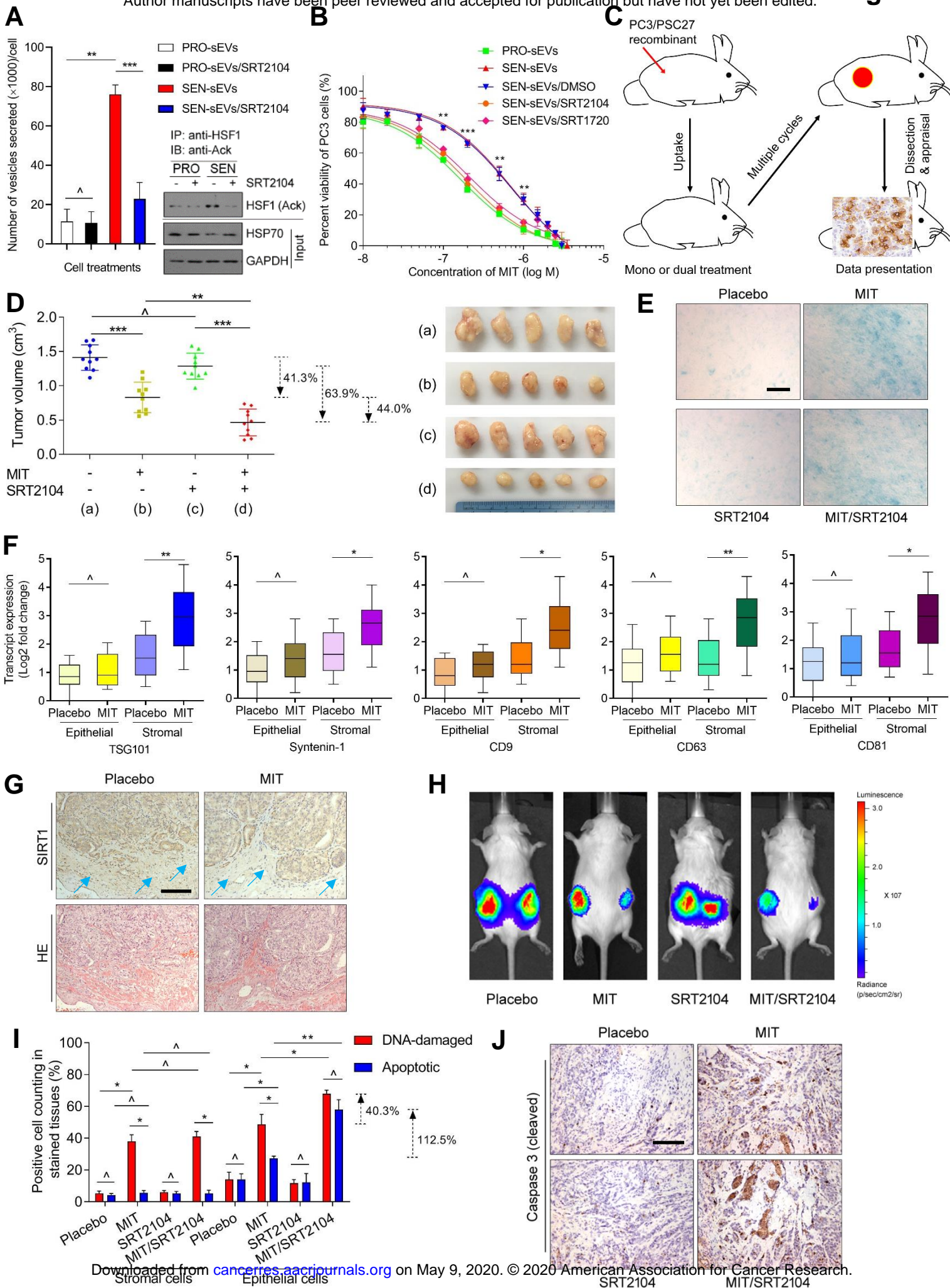
the impact of senescent stromal sEVs on development of therapeutic resistance of cancer cells in a TME niche.

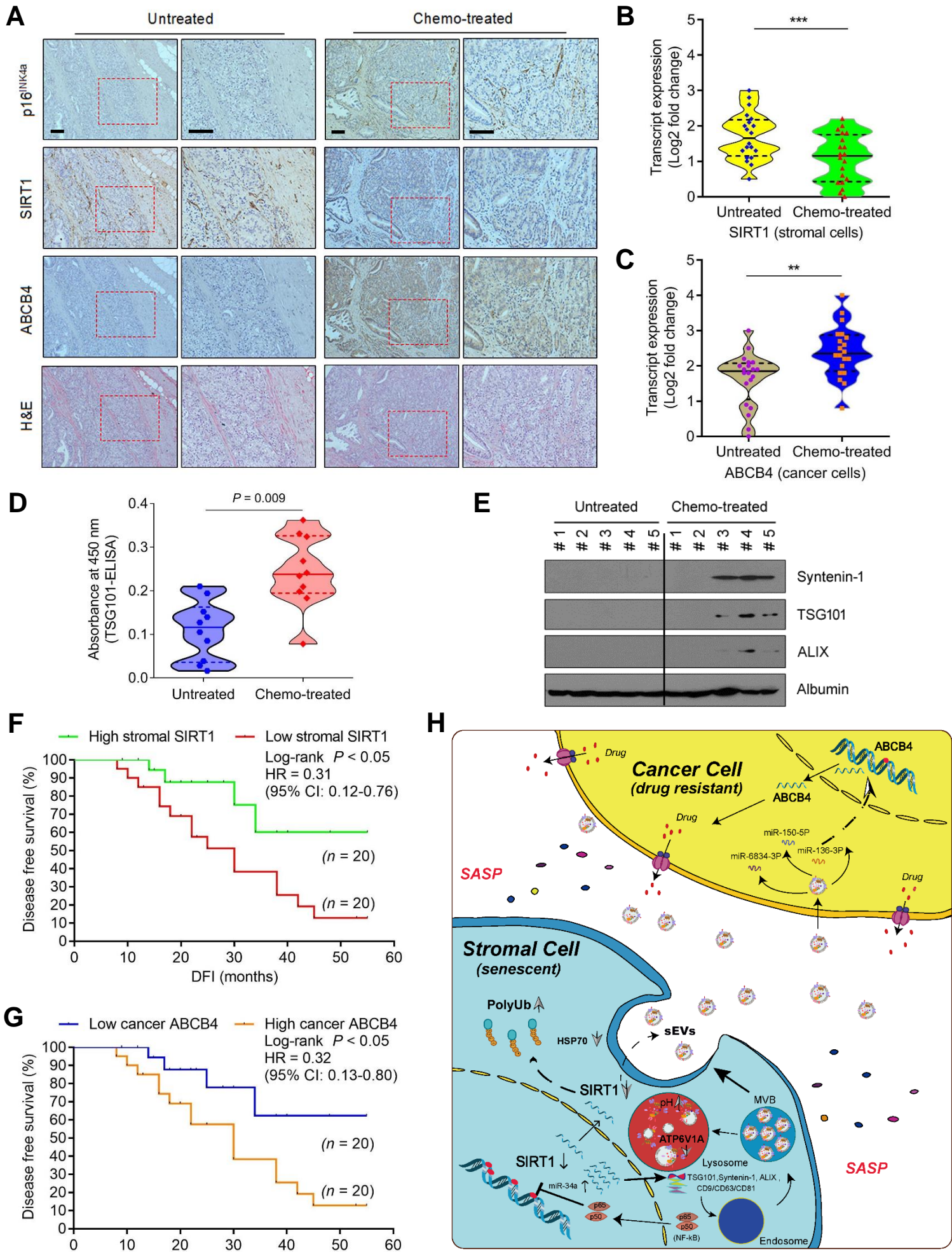


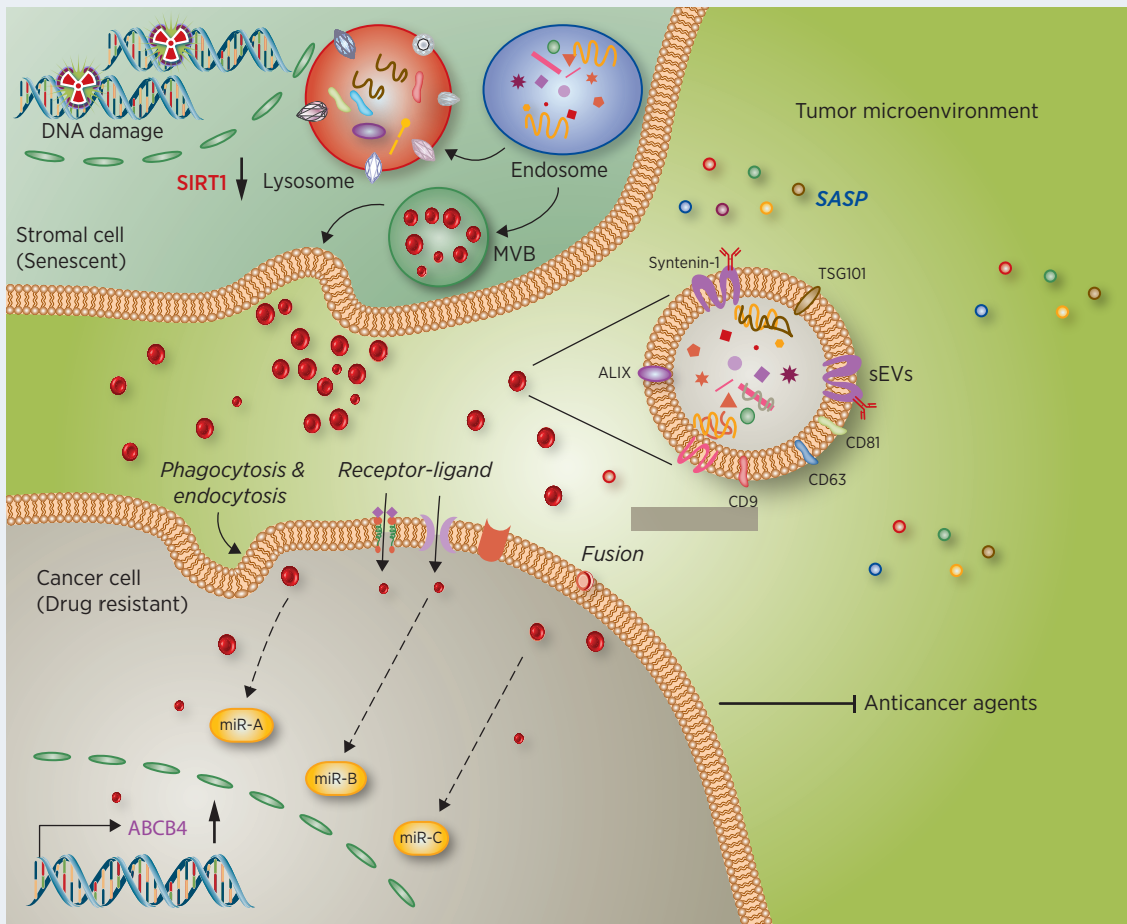












Senescent stromal cells produce small extracellular vesicles (sEVs) to promote cancer resistance in therapeutic settings, a process correlated with SIRT1 loss in stromal cells and ABCB4 expression in cancer cells. Downloaded from cancerres.aacrjournals.org on May 9, 2020. © 2020 American Association for Cancer Research.

Cancer Research

The Journal of Cancer Research (1916–1930) | The American Journal of Cancer (1931–1940)

Senescent stromal cells promote cancer resistance through SIRT1 loss-potentiated overproduction of small extracellular vesicles

Liu Han, Qilai Long, Shenjun Li, et al.

Cancer Res Published OnlineFirst May 4, 2020.

Updated version	Access the most recent version of this article at: doi: 10.1158/0008-5472.CAN-20-0506
Supplementary Material	Access the most recent supplemental material at: http://cancerres.aacrjournals.org/content/suppl/2020/05/02/0008-5472.CAN-20-0506.DC1
Author Manuscript	Author manuscripts have been peer reviewed and accepted for publication but have not yet been edited.

E-mail alerts	Sign up to receive free email-alerts related to this article or journal.
Reprints and Subscriptions	To order reprints of this article or to subscribe to the journal, contact the AACR Publications Department at pubs@aacr.org .
Permissions	To request permission to re-use all or part of this article, use this link http://cancerres.aacrjournals.org/content/early/2020/05/02/0008-5472.CAN-20-0506 . Click on "Request Permissions" which will take you to the Copyright Clearance Center's (CCC) Rightslink site.